Photoluminescence of spherical quantum dots

V. M. Fomin,* V. N. Gladilin,* and J. T. Devreese†
Theoretische Fysica van de Vaste Stof, Departement Natuurkunde, Universiteit Antwerpen (U.I.A.), Universiteitsplein 1, B-2610 Antwerpen-Wilrijk, Belgium

E. P. Pokatilov, S. N. Balaban, and S. N. Klimin
Laboratory of Multilayer Structure Physics, Department of Theoretical Physics, State University of Moldova, Strada A. Mateevici, 60, MD-2009 Kishinev, Republic of Moldova

(Received 7 July 1997)

In order to interpret the phonon-assisted optical transitions in semiconductor quantum dots, a theory is developed comprising the exciton interaction with both adiabatic and Jahn-Teller phonons and also the external nonadiabaticity (pseudo-Jahn-Teller effect). The effects of nonadiabaticity of the exciton-phonon system are shown to lead to a significant enhancement of phonon-assisted transition probabilities and to multiphonon optical spectra that are considerably different from the Franck-Condon progression. The calculated relative intensity of the phonon satellites and its temperature dependence compare well with the experimental data on the photoluminescence of CdSe quantum dots, both colloidal and embedded in glass.
[S0163-1829(98)03104-X]

I. INTRODUCTION

Recently, there has been an increasing experimental interest in multiphonon photoluminescence[1–5] and Raman scattering[6–11] of nanosize quantum dots. Photoluminescence peaks due to phonon-assisted processes were observed in colloidal quantum dots (nanocrystals) under size-selective excitation.[1,2] Observation of multiphonon photoluminescence of quantum dots embedded in glass is complicated because of a quick trapping of holes onto the local surface levels.[12] Overlapping of photoluminescence bands related to recombination of the electron-hole pairs, which are present in different states localized at the surface, smears the features of the spectrum due to the phonon-assisted processes.[4,13] Distinct phonon-line progressions, which are caused by recombination of the electron-hole pairs in ''interior'' states of a quantum dot (i.e., the states spatially quantized due to the confinement potential), were observed in the fast components of photoluminescence of CdSe quantum dots embedded in glass[3,4] using time-resolved spectroscopy.

Existing attempts to interpret[4,5,7,14,15] the aforementioned experiments on the basis of the *adiabatic* theory of multiphonon transitions in deep centers by Pekar[16] and Huang and Rhys[17] meet considerable difficulties. In the framework of the adiabatic theory, the values of the Huang-Rhys parameter were obtained in Refs. 14 and 15 using a spherical model Hamiltonian for the electron-hole pair in a quantum dot[18–20] and taking into account the valence-band mixing. The values of the Huang-Rhys parameter obtained in this way appear to be significantly (by one to two orders of magnitude) smaller than those derived from experiment. This discrepancy is due to the fact that under a strong confinement the charge density of the electron-hole pair in the ground state is small everywhere in the quantum dot. In order to achieve agreement with the experimental data, additional mechanisms have been intuitively introduced, which ensure separation of the electron and hole charges in space: (i) additional built-in charge,[7,14,21] (ii) traps that would localize holes,[2] and (iii) different boundary conditions for electrons and holes.[6]

The main idea of the adiabatic approach consists in the assumption that a stationary state of charge carriers is formed for each *instantaneous* position of ions (i.e., charge carriers follow the ion motion adiabatically). In the framework of this approach, the exciton-phonon interaction leads only to a modification of the exciton wave function, but does not give rise to transitions between different exciton states. However, two circumstances are to be mentioned, which imply that the exciton-phonon systems in quantum dots are essentially nonadiabatic.

(i) The states of an exciton in a quantum dot including the ground state are, generally speaking, *degenerate*. In this connection, it is worthwhile to recall,[22–26] that the electron-vibrational interaction in the impurity centers with a degenerate electron level may cause a dynamic Jahn-Teller effect,[27] or, equivalently, so-called *internal nonadiabaticity*. Namely, if the electron interaction with some vibrational modes is described by noncommutative matrices calculated in the basis of a degenerate electron level (those vibrational modes are usually called the nonadiabatic or Jahn-Teller modes), there is a nonadiabatic mixing of electron states belonging to this level. In a direct analogy to this scenario of the proper Jahn-Teller effect for the impurity centers, transitions do occur between different states of a degenerate exciton level in a quantum dot, provided the exciton-phonon interaction in the basis of this degenerate level is characterized by noncommutative matrices.

(ii) Differences between energy levels of an exciton in a quantum dot can become comparable to the optical phonon energy in the experiments.[1–10] Therefore, the resulting effects of *external nonadiabaticity*, or the so-called pseudo-Jahn-Teller effect,[26] in the phonon-assisted optical transitions are of crucial importance. The term ''external nonadiabaticity'' is used in order to make a distinction be-

tween this class of nonadiabatic phenomena and the above-described proper Jahn-Teller effect relevant to a degenerate exciton level.

To the best of our knowledge, in the papers on optical spectra of quantum dots, the effects of *nonadiabaticity* have been ignored when drawing an analogy between impurity centers, on the one hand, and quantum dots, on the other hand. In order to adequately describe the multiphonon optical spectra of quantum dots, it is necessary[28] to develop the nonadiabatic approach. This is the main goal of the present work.

The paper is organized as follows. In Sec. II the multiphonon light absorption by quantum dots is studied, taking into account the nonadiabaticity of the exciton-phonon system. It is demonstrated that the exciton interaction with the nonadiabatic vibration modes leads to a significant increase of multiphonon transition probabilities and to another dependence of these probabilities on the number of emitted or absorbed phonons as compared to the results of the theory of Pekar and of Huang and Rhys. Section III deals with the photoluminescence spectra of the ensemble of quantum dots. Two limiting cases are analyzed: the thermodynamic equilibrium photoluminescence that takes place when the time of the relaxation between the exciton energy levels is much smaller than the radiative lifetime of an exciton and the photoluminescence relevant to the slow relaxation. Section IV is devoted to the description of the model of the exciton-phonon systems in quantum dots used. In Sec. V the numerical results for the multiphonon photoluminescence spectra are displayed in comparison with the experimentally detected spectra of spherical CdSe quantum dots. It is emphasized that a straightforward calculation in the framework of the adiabatic theory gives the intensities of the phonon satellites that do not fit well the observed spectrum at any value of the Huang-Rhys parameter. Hence, as summarized in Sec. VI, the nonadiabaticity of the exciton-phonon systems is shown to play a crucial role in the phonon-assisted optical transitions in quantum dots.

II. LIGHT ABSORPTION BY QUANTUM DOTS

Quantum dots are considered to be embedded in a medium with a weak dispersion of refractive index. In this section the quantum dots are supposed to be identical. On the basis of the Kubo formula,[29] the linear coefficient of absorption by an ensemble of quantum dots in the electric dipole approximation[30] can be represented as

$$\alpha(\Omega)=\frac{8\pi\Omega\mathcal{N}}{3\hbar c n(\Omega)}(1-e^{-\hbar\Omega/k_BT}) \times \mathrm{Re}\int_0^\infty dt e^{i(\Omega+i\epsilon)t}\langle e^{(i/\hbar)Ht}d^\dagger e^{-(i/\hbar)Ht}d\rangle, \quad \epsilon\to 0^+, \tag{1}$$

where Ω is the light frequency, $\mathcal{N}$ is the concentration of quantum dots, $n(\Omega)$ is the refractive index of the medium, d is the dipole moment operator, and $\langle\ \rangle$ denotes the averaging over the statistical ensemble of the exciton-phonon systems. The total Hamiltonian of the exciton-phonon system

$$H=H_{ex}+H_{ph}+H_{int} \tag{2}$$

contains the exciton Hamiltonian H_{ex}, the phonon Hamiltonian H_{ph}, and the exciton-phonon interaction Hamiltonian

$$H_{int}=\sum_\lambda\ (\gamma_\lambda a_\lambda+\gamma_\lambda^\dagger a_\lambda^\dagger), \tag{3}$$

where $a_\lambda^\dagger$ and a_λ are the creation and annihilation operators for the phonons of the λth vibrational mode; the interaction operators γ_λ will be specified below.

Note that in the experiments,[1–5] the exciton energy is much larger than both the phonon energy and the value k_BT. This means, in particular, that the probability of thermal generation of an exciton is vanishing. For optical transitions leading to generation of an exciton and starting from the exciton vacuum $|0\rangle$ whose energy is chosen as zero, the initial states of the exciton-phonon system are described by the wave functions $|0\rangle|n\rangle$, where $|n\rangle$ are eigenstates of the phonon Hamiltonian H_{ph}. Further, the final states of the exciton-phonon system are not occupied, so that in Eq. (1), one can omit the term that is proportional to $\exp(-\hbar\Omega/k_BT)$ and describes a correction due to stimulated emission of light with frequency Ω. Finally, the frequency of the exciting radiation is much larger than the phonon frequency; hence the interaction of this radiation with free phonons can be neglected, i.e., $d|n\rangle=|n\rangle d$. Hence the transformation of the average follows:

$$\begin{aligned}\langle e^{(i/\hbar)Ht}d^\dagger e^{-(i/\hbar)Ht}d\rangle &= \sum_n\ \rho_n\langle n|e^{(i/\hbar)H_{ph}t}\langle 0|d^\dagger e^{-(i/\hbar)Ht}d|0\rangle|n\rangle \\ &= \langle 0|d^\dagger|\beta\rangle\langle\beta|\left(\sum_n\ \rho_n\langle n|e^{(i/\hbar)H_{ph}t}e^{-(i/\hbar)Ht}|n\rangle\right) \\ &\quad\times|\beta'\rangle\langle\beta'|d|0\rangle,\end{aligned} \tag{4}$$

where $|\beta\rangle$ labels eigenstates of the exciton Hamiltonian, ρ_n is the probability of the phonon state $|n\rangle$ in the equilibrium statistical ensemble of the phonon systems

$$\rho_n=\frac{1}{\mathcal{Z}_{ph}}\exp\left(-\frac{\mathcal{E}_n}{k_BT}\right),$$

$\mathcal{Z}_{ph}$ is the partition function of the free phonon subsystem, and $\mathcal{E}_n$ is the energy of the phonon state $|n\rangle$. Using the well-known Feynman relations[31] for operator exponentials, one obtains

$$e^{(i/\hbar)H_{ph}t}e^{-(i/\hbar)Ht}=e^{-(i/\hbar)H_{ex}t}U(t), \tag{5}$$

where the evolution operator

$$U(t)=T\exp\left(-\frac{i}{\hbar}\int_0^t dt_1 H_{int}(t_1)\right) \tag{6}$$

is represented in terms of the chronological ordering operator T, while

$$A(t)=e^{(i/\hbar)(H_{ex}+H_{ph})t}Ae^{-(i/\hbar)(H_{ex}+H_{ph})t}$$

denotes the operator A in the interaction representation. Hence Eq. (1) takes the form

$$\alpha(\Omega)=\frac{8\pi\Omega\mathcal{N}}{3\hbar cn(\Omega)}\mathrm{Re}\sum_{\beta,\beta'} d_\beta^* d_{\beta'} \times\int_0^\infty dt e^{i(\Omega-\Omega_\beta+i\epsilon)t}\langle\beta|\langle U(t)\rangle_{ph}|\beta'\rangle, \quad (7)$$

where Ω_β is the Franck-Condon frequency of generation of an exciton in the state $|\beta\rangle$, $d_\beta\equiv\langle\beta|d|0\rangle$ is the dipole matrix element of a transition between the exciton vacuum state and the state $|\beta\rangle$, and

$$\langle\ \rangle_{ph}\equiv\sum_n \rho_n\langle n|\ |n\rangle$$

denotes the averaging over the phonon ensemble.

Using Eq. (3) and neglecting the dispersion of the frequency of the optical phonons ω_0, one obtains the following result of the averaging over the equilibrium phonon ensemble in Eq. (7):

$$\langle U(t)\rangle_{ph}=T\exp\left\{-\frac{1}{\hbar^2}\sum_\lambda \int_0^t dt_1\int_0^{t_1} dt_2 \times[(\overline{n}+1)e^{-i\omega_0(t_1-t_2)}\gamma_\lambda(t_1)\gamma_\lambda^\dagger(t_2) + \overline{n}e^{i\omega_0(t_1-t_2)}\gamma_\lambda^\dagger(t_1)\gamma_\lambda(t_2)]\right\}, \quad (8)$$

where

$$\overline{n}=(e^{\hbar\omega_0/k_BT}-1)^{-1}. \quad (9)$$

The absorption coefficient $\alpha(\Omega)$ of Eq. (7) with Eq. (8) can be analytically calculated at arbitrary exciton-phonon coupling when (i) the exciton levels are nondegenerate (this case was analyzed by Pekar[16] and Huang and Rhys[17]) or (ii) the vibrational modes interacting with an exciton are adiabatic, i.e., the matrices $\|\langle\beta|\gamma_\lambda|\beta'\rangle\|$ in the basis of the degenerate level can be simultaneously diagonalized (this case is referred to as a static Jahn-Teller effect[22–25]).

However, these analytical approaches cannot be applied for the exciton-phonon systems in quantum dots because these systems are essentially nonadiabatic, as already stated in the Introduction. The fact that the exciton-phonon interaction in quantum dots is weak enables one to adequately describe the effect of the nonadiabaticity on phonon-assisted optical transitions. Here we will concentrate on the intensity of phonon satellites in the optical spectra; the influence of the Jahn-Teller effect on the energy spectrum of the system will be considered elsewhere.

Under the condition of weak exciton-phonon interaction

$$\eta\equiv\frac{\max|\langle\beta|\gamma_\lambda|\beta'\rangle|}{\hbar\omega_0}\ll 1, \quad (10)$$

contributions to the absorption coefficient from transitions, accompanied by a change of the number of phonons by K, can be calculated to leading (Kth) order in the small parameter η^2. In order to realize this approximation, it is enough to keep only those terms in the expansion of the evolution operator (8) where *all* the interaction operators $\gamma_\lambda(t)$ are placed either before or after *all* the operators $\gamma_\lambda^\dagger(t)$. Hence the absorption coefficient (7) takes the form

$$\alpha(\Omega)=\frac{8\pi\Omega\mathcal{N}}{3\hbar cn(\Omega)}\mathrm{Im}\left[\sum_{K=0}^\infty(\overline{n}+1)^K \times\sum_{\beta_{-K},\ldots,\beta_K}\varphi_K^{(+)}(\beta_{-K},\ldots,\beta_K;\Omega) + \sum_{K=1}^\infty\overline{n}^K\sum_{\beta_{-K},\ldots,\beta_K}\varphi_K^{(-)}(\beta_{-K},\ldots,\beta_K;\Omega)\right], \quad (11)$$

where β_i with $i=-K,\ldots,K$ label various intermediate and final exciton states relevant to the K-phonon optical transition; the other denotations are

$$\varphi_K^{(\pm)}(\beta_{-K},\ldots,\beta_K;\Omega) =\xi_K(\beta_{-K},\ldots,\beta_K) \times\prod_{k=-K}^K\frac{1}{\Omega_{\beta_k}\pm(K-|k|)\omega_0-\Omega-i\epsilon}, \quad (12)$$

$$\xi_0(\beta_0)=|d_{\beta_0}|^2, \quad (13)$$

$$\xi_K(\beta_{-K},\ldots,\beta_K)=\frac{d_{\beta_{-K}}^* d_{\beta_K}}{\hbar^{2K}}\sum_{n_1,\ldots,n_K=1}^K\prod_{i,i'=1}^K[1-\delta_{n_in_{i'}} \times(1-\delta_{ii'})]\prod_{k=1}^K\sum_\lambda\langle\beta_{-k}|\gamma_\lambda|\beta_{-k+1}\rangle \times\langle\beta_{n_k-1}|\gamma_\lambda^\dagger|\beta_{n_k}\rangle, \quad K\geqslant 1. \quad (14)$$

When the inequalities

$$|\Omega_\beta-\Omega_{\beta'}-k\omega_0|\gg\eta\omega_0 \quad (15)$$

are satisfied for any $|\beta\rangle$, $|\beta'\rangle$, and $k=1,2,3,\ldots$, the intensities of absorption lines can be expanded in powers of parameter η^2. To the leading (Kth) order in this parameter, the intensity of a line at the frequency $\Omega=\Omega_{\beta_0}\pm K\omega_0$ is determined by the residuum of the function $\varphi_K^{(\pm)}$ in the pole $\Omega=\Omega_{\beta_0}\pm K\omega_0+i\epsilon$. The residuum of the same function [see Eq. (12)] in each of the other $2K$ poles $\Omega=\Omega_{\beta_k}\pm(K-|k|)\omega_0+i\epsilon$ with $|k|\geqslant 1$ describes a relatively small correction $\sim\eta^{2K}$ to the $(K-|k|)$-phonon-line intensity determined by its leading term, which is of the order of $\eta^{2(K-|k|)}$.

Under the resonance conditions $|\Omega_\beta-\Omega_{\beta'}-k\omega_0|\to 0$ (where $k=1,2,3,\ldots$), the phonon-line intensities calculated within the framework of perturbation theory may diverge and hence a straightforward expansion of the absorption coefficient $\alpha(\Omega)$ in powers of η^2 is not adequate. The following procedure allows one to study the resonance situation too. The resonance situation is noticeable for the fact that the optical spectra contain groups of close spectral lines. Distinct phonon-line progressions can then be observed in the optical spectra of quantum dots provided that (i) for the frequencies

of optical transitions corresponding to one and the same νth group, with $\overline{\Omega}_\nu$ denoting the central position of spectral lines of this group, the inequalities

$$|\Omega_\beta \pm K\omega_0 - \overline{\Omega}_\nu| < \Delta\Omega/2, \quad \Delta\Omega \ll \omega_0, \quad K = 0,1,2,\ldots, \tag{16}$$

are fulfilled and (ii) the groups are separated from each other by relatively large frequency intervals

$$|\overline{\Omega}_{\nu'} - \overline{\Omega}_\nu| \gg \Delta\Omega, \quad \nu' \neq \nu. \tag{17}$$

For the νth group, the integer parameter K obeying the inequality (16) possesses a minimum value that is denoted as K_ν. If the interval $\Delta\Omega$ is chosen to be much larger than $\eta\omega_0$ [such a choice is always possible under condition (10)], the average absorption coefficient on the frequency interval $(\overline{\Omega}_\nu - \Delta\Omega/2, \overline{\Omega}_\nu + \Delta\Omega/2)$

$$\alpha_\nu = \frac{1}{\Delta\Omega}\int_{\overline{\Omega}_\nu - \Delta\Omega/2}^{\overline{\Omega}_\nu + \Delta\Omega/2} \alpha(\Omega')\, d\Omega' \tag{18}$$

can be expanded in powers of η^2 because the integration in Eq. (18) eliminates the problem of the above-mentioned divergences of the phonon-line intensities. The leading terms of such an expansion are determined by the residua of the functions $\varphi_{K_\nu}^{(\pm)}$ in the poles $\Omega = \Omega_{\beta_0} \pm K_\nu\omega_0 + i\epsilon$, the frequencies Ω_{β_0} satisfying the inequality (16) at $K = K_\nu$. As results from the definition of the parameter K_ν, all the other $2K_\nu$ poles $\Omega = \Omega_{\beta_k} \pm (K_\nu - |k|)\omega_0 + i\epsilon$ (with $|k| \geqslant 1$) of the function $\varphi_{K_\nu}^{(\pm)}$ lie far away from the interval $(\overline{\Omega}_\nu - \Delta\Omega/2, \overline{\Omega}_\nu + \Delta\Omega/2)$ and correspond already to other groups of spectral lines. In combination with inequalities (16) and (17), this leads to the following property of residua of the functions $\varphi_K^{(\pm)}$ (12): The residua determining the *leading terms* in the average absorption coefficient α_ν contain in their denominators no small factors that would obey the inequalities $|\Omega_\beta - \Omega_{\beta'} - k\omega_0| \leqslant \Delta\Omega$ (where $k = 1,2,3,\ldots$). This property implies, consequently, that the contributions to the average absorption coefficient due to the residua that contain small denominators of the aforementioned type can be neglected. Therefore, in order to correctly (within a relative accuracy $\sim \eta^2$) describe the values of the average absorption coefficient on the narrow frequency intervals $(\overline{\Omega}_\nu - \Delta\Omega/2, \overline{\Omega}_\nu + \Delta\Omega/2)$, the function $\alpha(\Omega)$ (11) should be represented as

$$\alpha(\Omega) = \frac{8\pi^2\Omega\mathcal{N}}{3\hbar c n(\Omega)} \sum_\beta \left[\sum_{K=0}^{\infty} (\overline{n}+1)^K f_{\beta K}^{(+)} \delta(\Omega_\beta + K\omega_0 - \Omega) + \sum_{K=1}^{\infty} \overline{n}^K f_{\beta K}^{(-)} \delta(\Omega_\beta - K\omega_0 - \Omega) \right]. \tag{19}$$

Here the coefficients $f_{\beta K}^{(+)}(f_{\beta K}^{(-)})$ defined by

$$f_{\beta 0}^{(\pm)} = |d_\beta|^2, \tag{20}$$

$$f_{\beta K}^{(\pm)} = \sum_{\beta_{-K},\ldots,\beta_K} \delta_{\beta_0\beta}\xi_K(\beta_{-K},\ldots,\beta_K) \prod_{k=1}^{K} \times \frac{\theta(|\Omega_{\beta\beta_k} \pm k\omega_0| - \Delta\Omega)\,\theta(|\Omega_{\beta\beta_{-k}} \pm k\omega_0| - \Delta\Omega)}{(\Omega_{\beta\beta_k} \pm k\omega_0)(\Omega_{\beta\beta_{-k}} \pm k\omega_0)}, \quad K \geqslant 1, \tag{21}$$

are proportional to the probabilities for the generation of an exciton in the state $|\beta\rangle$ with simultaneous emission (absorption) of K phonons,

$$\theta(x) = \begin{cases} 1, & x \geqslant 0, \\ 0, & x < 0, \end{cases} \tag{22}$$

$$\Omega_{\beta\beta'} = \Omega_\beta - \Omega_{\beta'}. \tag{23}$$

In Eq. (21), there are three kinds of terms which contain nondiagonal matrix elements $\langle\beta_i|\gamma_\lambda|\beta_k\rangle$ in the coefficients ξ_K: (i) terms with all the states $|\beta_{-K}\rangle, \ldots, |\beta_K\rangle$ belonging to the *same* energy level, which describe the influence of the internal nonadiabaticity (or the proper Jahn-Teller effect) on the optical transition probabilities; (ii) terms with $|\beta_{-K}\rangle, \ldots, |\beta_K\rangle$ pertaining to *different* energy levels, which take into account the effects of the external nonadiabaticity (or the so-called pseudo-Jahn-Teller effect); and (iii) terms proportional to $d^*_{\beta_{-K}} d_{\beta_K}$ with $\beta_{-K} \neq \beta_K$, which describe the *intermultiplet mixing* between the exciton states with the same symmetry. This mixing occurs due to the exciton-phonon interaction.

When an exciton energy level is degenerate, Eq. (21) differs from the result of the adiabatic theory,[16,17] which gives for a weak exciton-phonon interaction

$$\tilde{f}_{\beta K} = \frac{|d_\beta|^2}{K!}\left(\sum_\lambda \left| \frac{\langle\beta|\gamma_\lambda|\beta\rangle}{\hbar\omega_0} \right|^2 \right)^K, \tag{24}$$

the difference taking place even if one neglects the effects mentioned in points (ii) and (iii) above. For example, the shape of the absorption band edge of a spherical quantum dot can be obtained using the spherical model[18–20] for the exciton Hamiltonian (see the Appendix). The coefficients $f_{\beta K}^{(\pm)}$ that are proportional to the probabilities of generation of an exciton in the ground state with emission or absorption of K phonons of non-adiabatic (or, equivalently, Jahn-Teller) modes are then given by

$$\frac{f_{\beta K}^{(\pm)}}{\tilde{f}_{\beta K}} = \frac{4}{3}\left(\left[\frac{K+1}{2} \right] + \frac{1}{2} \right)\left(\left[\frac{K+1}{2} \right] + \frac{3}{2} \right), \tag{25}$$

where $[x]$ denotes the integer part of x. The adequate account of the exciton interaction with the Jahn-Teller vibrations leads to a significant increase of the multiphonon transition probabilities and to a more complicated dependence of these probabilities on the number of emitted or absorbed phonons in comparison with the results of the theory by Pekar[16] and Huang and Rhys.[17] Therefore, the multiphonon optical spectrum determined by Eq. (19) with Eq. (25) is

considerably different from the Franck-Condon progression described by Eq. (19), where the $f_{\beta K}^{(\pm)}$ are replaced by the $\tilde{f}_{\beta K}$ given through Eq. (24).

III. PHOTOLUMINESCENCE SPECTRUM

The relaxation processes during the time interval t between the generation and the recombination of an exciton substantially influence the photoluminescence spectrum. Two limiting cases are examined here: (i) the thermodynamic equilibrium photoluminescence that takes place when τ_0 the time of the relaxation between the exciton energy levels is much smaller than the radiative lifetime of an exciton τ and (ii) the opposite case relevant to slow relaxation $\tau_0 \gg \tau$. The energy level broadening due to the finite values of τ_0 and τ is disregarded here, i.e., the inequalities $\tau_0^{-1}, \tau^{-1} \ll \omega_0$ are supposed to be satisfied. This supposition is in agreement with the theoretical estimations of the exciton lifetime (for example, the value $\tau \sim 1$ ns was obtained in Ref. 4 for CdSe quantum dots) and with the experimental observation of ultranarrow (<0.15 meV) luminescence lines from *single* quantum dots.[32] The spectral broadening of the multiphonon photoluminescence lines will be considered below in Sec. V.

According to Refs. 24 and 33, the spectrum of equilibrium luminescence can be obtained directly from the absorption spectrum. For an ensemble of identical quantum dots, the equilibrium-luminescence intensity can be expressed as

$$I(\Omega)=\frac{\hbar\Omega^3 n^2(\Omega)}{2\pi^2 c^2}\frac{\mathcal{N}_{ex}}{\mathcal{N}}\frac{\mathcal{Z}_{ph}}{\mathcal{Z}}\exp\left(-\frac{\hbar\Omega}{k_B T}\right)\alpha(\Omega), \quad (26)$$

where the partition function $\mathcal{Z}$ relates to the states of the system that includes one exciton and phonons. The concentration of excited quantum dots $\mathcal{N}_{ex}$ is described by

$$\mathcal{N}_{ex}=\frac{s\,\alpha(\Omega_{exc})\mathcal{I}_{exc}}{\hbar\Omega_{exc}}, \quad (27)$$

where Ω_{exc} and $\mathcal{I}_{exc}$ are the frequency and the intensity of the monochromatic exciting radiation; the factor $s=\tau$ for the continuous excitation, while $s=\tau_{exc}\exp(-t/\tau)$ for the excitation by short light pulses of duration $\tau_{exc} \ll \tau$. Substituting the equation for α (19) in Eqs. (26) and (27), one obtains at low temperatures typical for the experiments[1–5] ($k_B T \ll \hbar\omega_0$)

$$I(\Omega)=\mathcal{N}\sum_{K=0}^{\infty}\sum_{\beta,\beta'}\delta(\Omega-\Omega_{exc}+K\omega_0+\Omega_{\beta'\beta}) \times\sum_{K'=0}^{K}A_{\beta\beta' KK'}\delta(\Omega_{exc}-\Omega_{\beta'}-K'\omega_0), \quad (28)$$

where

$$A_{\beta\beta' KK'}=\frac{32\pi^2\Omega^4 s\mathcal{I}_{exc}}{9\hbar^2 c^4\mathcal{Z}_{ex}}\exp\left(-\frac{\hbar\Omega_\beta}{k_B T}\right)f_{\beta,K-K'}^{(-)}f_{\beta' K'}^{(+)}, \quad (29)$$

with $\mathcal{Z}_{ex}$ the partition function of the one-exciton subsystem. When deriving Eq. (29) it was taken into account that within the framework of the weak-coupling approach developed in Sec. II, $\mathcal{Z}\approx\mathcal{Z}_{ex}\mathcal{Z}_{ph}$. In the limit of slow relaxation $\tau_0 \gg \tau$, the recombination occurs from a state in which an exciton has been generated, hence the photoluminescence intensity follows from Eq. (19) to be

$$I(\Omega)=\mathcal{N}\sum_{K=0}^{\infty}\delta(\Omega-\Omega_{exc}+K\omega_0)\sum_{\beta}\sum_{K'=0}^{K}B_{\beta KK'} \times\delta(\Omega_{exc}-\Omega_\beta-K'\omega_0), \quad (30)$$

where

$$B_{\beta KK'}=\frac{32\pi^2\Omega^4 s_\beta\mathcal{I}_{exc}}{9\hbar^2 c^4}f_{\beta,K-K'}^{(-)}f_{\beta K'}^{(+)}, \quad (31)$$

with the factors s_β described at $\tau_{exc} \ll \tau$ by

$$s_\beta=\tau_{exc}\exp\left\{-\frac{4t}{\hbar c^3}\sum_{K=0}^{\infty}(\Omega_\beta-K\omega_0)^3 n(\Omega_\beta-K\omega_0)f_{\beta K}^{(-)}\right\}. \quad (32)$$

For a specimen that contains quantum dots of different types the photoluminescence intensities (28) and (30) must be summed up over those different types. When one considers an ensemble of spherical quantum dots with a continuous distribution function $\mathcal{N}(R)$ over the radii R, the aforementioned summation is realized by an integration over radii. For the equilibrium-photoluminescence intensity one then obtains from Eq. (28)

$$I(\Omega)=\sum_{K=0}^{\infty}\sum_{K'=0}^{K}\sum_{\beta,\beta'}\mathcal{N}(R_{\beta' K'})A_{\beta\beta' KK'}(R_{\beta' K'}) \times\delta(\Omega-\Omega_{exc}+K\omega_0+\Omega_{\beta'\beta}(R_{\beta' K'})), \quad (33)$$

while in the opposite limit $\tau_0 \gg \tau$ the photoluminescence intensity of Eq. (30) takes the form

$$I(\Omega)=\sum_{K=0}^{\infty}\delta(\Omega-\Omega_{exc}+K\omega_0) \times\sum_{K'=0}^{K}\sum_{\beta}\mathcal{N}(R_{\beta K'})B_{\beta KK'}(R_{\beta K'}). \quad (34)$$

The monochromatic excitation light with frequency Ω_{exc} is absorbed only by quantum dots of radii $R_{\beta' K'}$ satisfying the equation

$$\Omega_{\beta'}(R)+K'\omega_0-\Omega_{exc}=0. \quad (35)$$

The photoluminescence spectrum described by Eq. (34) contains only one phonon-line progression with a zero-phonon line at the frequency $\Omega=\Omega_{exc}$, while the equilibrium-photoluminescence spectrum consists of a set of phonon-line progressions shifted from Ω_{exc} by the values $\Omega_{\beta\beta'}$ (23), which are determined by exciton energy losses due to the radiationless relaxation. The schemes of the relevant optical transitions in quantum dots are shown in Fig. 1. In particular, the equilibrium-photoluminescence line at the frequency $\Omega=\Omega_{exc}-K\omega_0-\Omega_{\beta'\beta}(R_{\beta' K'})$ corresponds to the following sequence of transitions in a quantum dot of

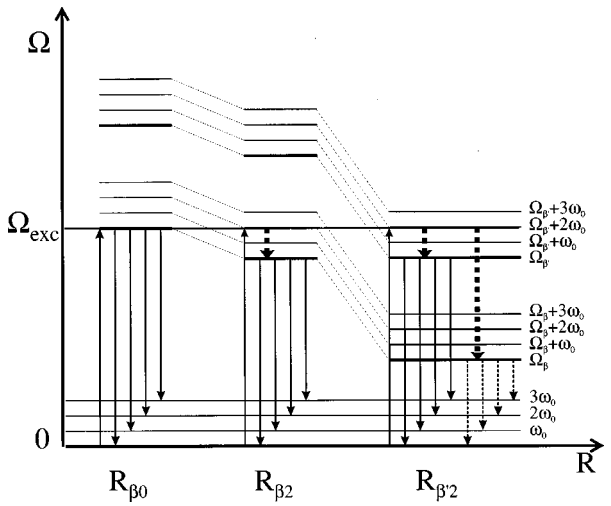

FIG. 1. Scheme of the transitions for the light absorption under the excitation by the radiation of frequency Ω_{exc} (arrows up) and for the subsequent luminescence (arrows down) in quantum dots of three different radii. Radiationless transitions are shown by heavy dashed lines. Thin dashed lines indicate a phonon-line progression occurring in the photoluminescence spectrum after the exciton relaxation from the state $|\beta'\rangle$ into the state $|\beta\rangle$. The values ω_0 and $\Omega_{\beta'}-\Omega_{\beta}$ are shown magnified as compared to the frequency Ω_{exc}.

radius $R_{\beta' K'}$ (e.g., of radius $R_{\beta' 2}$ in Fig. 1): (i) generation of an exciton in the state $|\beta'\rangle$ accompanied by emission of $K'(K' \leqslant K)$ phonons (shown by arrow up), (ii) radiationless transition of the exciton to the state $|\beta\rangle$ (heavy dashed arrow), and (iii) radiative recombination of the exciton with emission of $K-K'$ phonons (thin dashed arrows for transitions with emission of zero to three phonons).

IV. MODELS FOR QUANTUM DOTS

Both the quantum dots in glass and the colloidal quantum dots of small size (1–2 nm) are known[2–5] to have a geometrical shape close to spherical. For the samples investigated in Refs. 3 and 4, small-angle x-ray measurements have indicated that the function $\mathcal{N}(R)$ that describes the distribution of quantum dots over radii is close to the logarithmic standard distribution

$$\mathcal{N}(R)=\frac{\mathcal{N}_{tot}}{\sqrt{2\pi}\varrho R}\exp\left\{-\left[\frac{\ln(R/R_0)}{\sqrt{2}\varrho}\right]^2\right\}, \tag{36}$$

the average radius of quantum dots being determined as

$$\langle R\rangle = R_0\exp\left(\frac{\varrho^2}{2}\right). \tag{37}$$

Here R_0 and ϱ are distribution parameters and $\mathcal{N}_{tot}$ is the total concentration of quantum dots

$$\mathcal{N}_{tot}=\int_0^\infty \mathcal{N}(R)dR.$$

In Sec. V the function $\mathcal{N}(R)$ (36) is used to model the distribution of quantum dots over radii.

In the exciton-phonon interaction Hamiltonian H_{int} (3), the operators γ_λ are

$$\gamma_\lambda=\gamma_\lambda(\mathbf{r}_e)-\gamma_\lambda(\mathbf{r}_h), \tag{38}$$

where $\mathbf{r}_e$ and $\mathbf{r}_h$ are the coordinates of an electron and a hole, respectively. In a spherical quantum dot the interaction operators $\gamma_\lambda^B(\mathbf{r})$ and $\gamma_\lambda^I(\mathbf{r})$ describing the electron interaction, respectively, with the bulk and interface phonons are expressed according to Ref. 34 by

$$\gamma_\lambda^{(B)}(\mathbf{r})\equiv\gamma_{nlm}^{(B)}(\mathbf{r})=v_{nl}^{(B)}(r)i^{-l-m-|m|}Y_{lm}(\vartheta,\varphi), \tag{39}$$

$$\gamma_\lambda^{(I)}(\mathbf{r})\equiv\gamma_{lm}^{(B)}(\mathbf{r})=v_{l}^{(I)}(r)i^{-l-m-|m|}Y_{lm}(\vartheta,\varphi), \tag{40}$$

where $Y_{lm}(\vartheta,\varphi)$ are the spherical harmonics. The radial parts of the interaction operators are described by

$$v_{nl}^{(B)}(r)=e\sqrt{\frac{\hbar\omega_0}{\epsilon_0 R}\left(\frac{1}{\epsilon(\infty)}-\frac{1}{\epsilon(0)}\right)}\frac{j_l(z_{ln}r/R)}{z_{ln}j_l'(z_{ln})}, \tag{41}$$

$$v_{l}^{(I)}(r)=e\sqrt{\frac{\hbar\omega_0}{\epsilon_0 R}\left(\frac{1}{\epsilon(\infty)}-\frac{1}{\epsilon(0)}\right)}\frac{\sqrt{l}\,\epsilon(\infty)}{l\epsilon(\infty)+(l+1)\widetilde{\epsilon}(\infty)}\left(\frac{r}{R}\right)^l, \tag{42}$$

where $j_l(z)$ are the spherical Bessel functions, z_{ln} is the nth zero of the function $j_l(z)$, ϵ_0 is the permittivity of vacuum, $\epsilon(\infty)$ and $\widetilde{\epsilon}(\infty)$ are the optical dielectric constants, respectively, of a quantum dot and of its surrounding medium, and $\epsilon(0)$ is the static dielectric constant of a quantum dot.

The exciton Hamiltonian for the spherical model[18–20] supplemented to account for the electron-hole exchange interaction[35,36] is

$$H_{ex}=\frac{1}{2m_e}\mathbf{p}_e^2+\frac{\gamma_1}{2m_0}\mathbf{p}_h^2-\frac{\gamma_2}{9m_0}(\mathbf{P}^{(2)}\cdot\mathbf{J}^{(2)})+V_C(\mathbf{r}_e,\mathbf{r}_h)$$
$$-\frac{2}{3}\varepsilon_{exch}a_0^3\delta(\mathbf{r}_e-\mathbf{r}_h)(\boldsymbol{\sigma}\cdot\mathbf{J}). \tag{43}$$

Here $\mathbf{p}_e$ and $\mathbf{p}_h$ are the momenta of an electron and a hole, respectively, γ_1 and γ_2 are the Luttinger parameters, $\mathbf{P}^{(2)}$ and $\mathbf{J}^{(2)}$ are the irreducible second-rank tensor operators of the momentum and the spin-$\frac{3}{2}$ angular momentum of a hole, $\boldsymbol{\sigma}$ and $\mathbf{J}$ are the spin operators of an electron and a hole, a_0 is the lattice constant, and ε_{exch} is the exchange strength constant,[37] which is equal to 320 meV in CdSe.[36] In a spherical quantum dot, the Coulomb electron-hole interaction may be approximately described by the Hamiltonian[34]

$$V_C(\mathbf{r}_e,\mathbf{r}_h)=-\frac{e^2}{4\pi\epsilon_0\epsilon(\infty)}\sum_{l=0}^{\infty}P_l(\cos\vartheta_{eh})$$
$$\times\left\{\frac{r_e^l}{r_h^{l+1}}\theta(r_h-r_e)+\frac{r_h^l}{r_e^{l+1}}\theta(r_e-r_h)\right.$$
$$\left.+\frac{(r_e r_h)^l}{R^{2l+1}}\frac{[\epsilon(\infty)-\widetilde{\epsilon}(\infty)](l+1)}{\epsilon(\infty)+\widetilde{\epsilon}(\infty)(l+1)}\right\}, \tag{44}$$

where $P_l(x)$ is a Legendre polynomial of degree l and ϑ_{eh} is the angle between $\mathbf{r}_e$ and $\mathbf{r}_h$. The Franck-Condon frequency

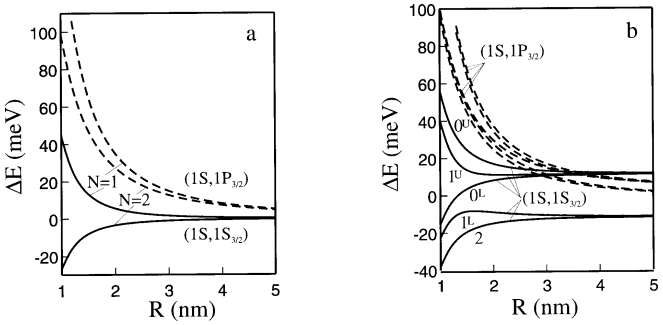

FIG. 2. Lowest-energy levels of an exciton in a spherical CdSe quantum dot as a function of the radius. (a) Splitting of the energy levels due to the electron-hole exchange interaction in quantum dots with zinc-blende (cubic) structure. (b) Splitting of the energy levels due to both the exchange interaction and anisotropic crystal field in quantum dots with wurtzite (hexagonal) structure. The degenerate level $(1S,1S_{3/2})$ is chosen as the origin of the energy scale.

for generation of an exciton in the eigenstate $|\beta\rangle$ is determined by the corresponding eigenvalue $\mathcal{E}_\beta$ of the Hamiltonian (43) as

$$\Omega_\beta=\frac{E_g+\mathcal{E}_\beta}{\hbar}, \tag{45}$$

where E_g is the energy band gap for the substance of the quantum dot.

For typical[2–4] quantum dot radii, the exciton states are determined mainly by confinement, while the electron-hole interaction can be treated as a perturbation. To zeroth order in this perturbation, the hole states,[20] designated as $nS_{3/2}$, $nP_{1/2}$, $nP_{3/2}$, $nP_{5/2}$, $nD_{1/2}$, $nD_{5/2}$, ... are characterized by definite values of the hole angular momentum $\mathbf{F}=\mathbf{L}+\mathbf{J}$ (where $\mathbf{L}$ is the orbital angular momentum of a hole) and the parity; n labels the solutions of the equations for the radial components of the hole wave function.[20]

Under size-selective excitation, the frequency Ω_{exc} is chosen to lie in the absorption band tail. Thus only the largest quantum dots are involved in the absorption processes and excitons are generated in the lowest states. The exciton ground state $(1S,1S_{3/2})$ and the state $(1S,1P_{3/2})$ separated from the ground state by an energy comparable to the phonon energy $\hbar\omega_0$ play the main role in the absorption and the photoluminescence. (As for an electron, the energy of its size quantization is large and only the state $1S$ must be taken into account.)

In a spherical quantum dot, both the energy level $(1S,1S_{3/2})$ and the level $(1S,1P_{3/2})$ are eightfold degenerate to the zeroth order in electron-hole interaction. In a quantum dot with zinc-blende structure, the electron-hole exchange interaction splits[35,36] each of these levels into a fivefold degenerate level with eigenvalue $N=2$ of the exciton angular momentum $\mathbf{N}=\boldsymbol{\sigma}+\mathbf{F}$ and a threefold degenerate level with $N=1$ [see Fig. 2(a)]. In a quantum dot with wurtzite structure, the crystal field, described by the potential[37]

$$V=-\frac{\Delta}{2}\left(J_z^2-\frac{1}{4}\right), \tag{46}$$

[where $\Delta=25$ meV for CdSe (Ref. 38) and J_z is the spin angular momentum component of a hole along the unique axis of hexagonal lattice], together with the electron-hole exchange interaction, leads[5,36] to the splitting of the level $(1S,1S_{3/2})$ into five sublevels with definite values of the exciton angular momentum components N_z along the crystal axis, as indicated in Fig. 2(b): a twofold degenerate level with $|N_z|=2$ (the curve with the label 2), two twofold degenerate levels with $|N_z|=1$ (two curves with the labels 1^L and 1^U for the lower and upper sublevels, respectively), and two nondegenerate levels with $|N_z|=0$ (two curves with the labels 0^L and 0^U). The splitting of the level $(1S,1P_{3/2})$ is characterized by relatively smaller energy intervals between sublevels [see Fig. 2(b)], while the mutual order of sublevels with different $|N_z|$ is the same as that for the level $(1S,1S_{3/2})$.

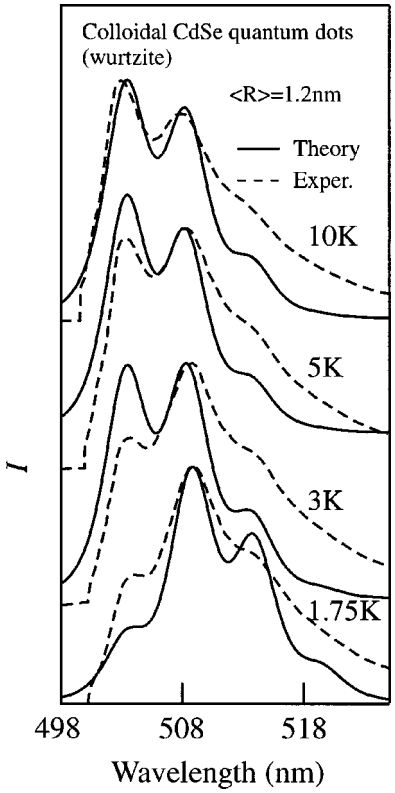

FIG. 3. Fluorescence spectra of CdSe quantum dots with wurtzite structure at various temperatures. Solid lines were calculated by using Eq. (33) and dashed lines represent the experimental data of Ref. 2. Different lines are shifted along the vertical axis for clarity.

In quantum dots with both the zinc-blende structure and the wurtzite structure, the zero-phonon generation of an exciton in the ground state and the radiative recombination from this state are forbidden in the dipole approximation. Therefore, the intensity of zero-phonon line is due to transitions from high-energy levels. As a consequence, on the basis of Eq. (33) combined with Eq. (29), a decrease of temperature must result in a decrease of the zero-phonon-line intensity in the equilibrium-luminescence spectra. Such a behavior is in agreement with the experimental data.[2]

V. NUMERICAL RESULTS AND COMPARISON WITH THE EXPERIMENT

In Figs. 3 and 4, the fluorescence spectra $I(\Omega)$ calculated by using Eq. (33) are presented together with the experimen-

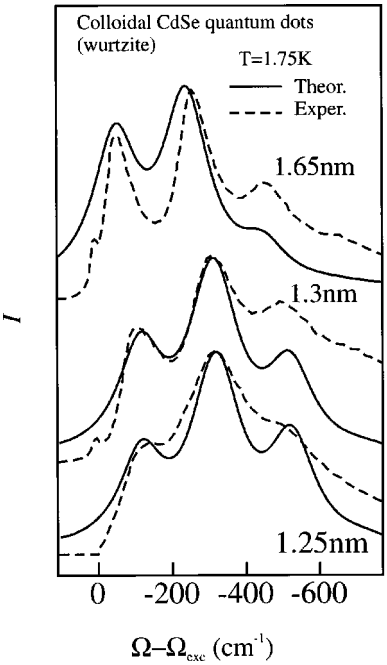

FIG. 4. Fluorescence spectra of CdSe quantum dots with wurtzite structure at various average radii $\langle R\rangle$. Solid lines were calculated by using Eq. (33) and dashed lines represent the experimental data of Ref. 2. Different lines are shifted along the vertical axis for clarity.

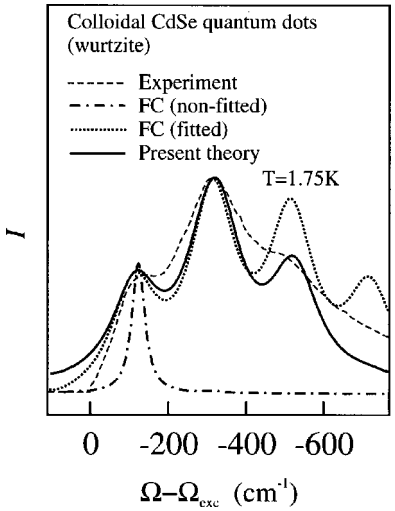

FIG. 5. Fluorescence spectra of CdSe quantum dots with wurtzite structure at the average radius $\langle R\rangle = 1.25$ nm. The dashed line represents the experimental data of Ref. 2, the dot-dashed line displays a Franck-Condon progression with the Huang-Rhys parameter $S = 0.06$ calculated in Ref. 14, the dotted line shows another Franck-Condon progression with the Huang-Rhys parameter $S = 1.7$, which is obtained by fitting the ratio of one-phonon and zero-phonon peak heights to the experimental value, and the solid line results from the calculation by using Eq. (33).

tal data of Ref. 2 on colloidal CdSe quantum dots of wurtzite structure, respectively, at different temperatures T and average radii $\langle R\rangle$. The following values of the parameters were used: $\epsilon(\infty)=6.23$, $\epsilon(0)=9.56$, $m_e=0.13m_0$, and $E_g = 1.75$ eV from Ref. 14 and $\gamma_1=2.04$ and $\gamma_2=0.58$ from Ref. 39. From a comparison of the calculated absorption spectrum (19) with the experimental absorption spectrum of Ref. 2, the value 0.06 was obtained for the parameter ϱ of the distribution function $\mathcal{N}(R)$ (36). Because of the chaotic nature of the energy spectrum of excitons in real quantum dots (e.g., owing to the strain or nonperfect geometrical form) and also due to a limited spectral resolution of experimental equipment, photoluminescence lines described by δ functions turn into broadened peaks. The shape of these peaks was modeled by Lorentzians of finite width $\Gamma = 15$ meV.

It is worthwhile to note that in CdSe quantum dots of wurtzite structure, the magnitude of the $(1S,1S_{3/2})$-level splitting by the crystal field for a wide range of radii R is close to the optical phonon energy $\hbar\omega_0=25$ meV as seen from Fig. 2(b). Therefore, the observed peak of the equilibrium photoluminescence in the spectral region $\Omega\approx\Omega_{exc} - K\omega_0$ is caused not only by K-phonon processes (with probability $\sim\eta^{2K}$), but also by $(K-1)$-phonon processes (with probability $\sim\eta^{2(K-1)}$). The latter processes are related to the generation of an exciton in the *upper* group of states [resulting from the splitting of the $(1S,1S_{3/2})$ level] and the subsequent radiationless relaxation to the *lower* group of states. This feature of the energy spectrum of the exciton-phonon system in quantum dots, in combination with the pseudo-Jahn-Teller effect, leads to a substantial difference of the observed spectrum of multiphonon photoluminescence from the Franck-Condon progression, as shown in Fig. 5. It is important to note that a straightforward calculation in the framework of the adiabatic theory leads to intensities of the phonon satellites that do not fit the observed spectrum well for any value of the Huang-Rhys parameter.

In Fig. 6(a)–6(d) the photoluminescence spectra $I(\Omega)$ calculated for a zinc-blende-type crystal lattice are given and compared with the experimental data of Ref. 4 on photoluminescence of CdSe quantum dots in borosilicate glass. The parameter values $m_e=0.11m_0$ and $E_g=1.9$ eV (Ref. 40) were used for the zinc-blende lattice. The theoretical curves are calculated for the time interval between generation and recombination of an exciton $t\ll\tau$. The shape of photoluminescence peaks was modeled by Lorentzians of width $\Gamma = 2$ meV relevant to the limited spectral resolution of measurements (better than 5 meV in Ref. 4). From a comparison of the calculated absorption spectra (19) with the experimental absorption spectra of Ref. 4 the values 0.15, 0.18, and 0.20 of the parameter ϱ were obtained for average radii $\langle R\rangle$ equal to 1.4 nm, 1.8 nm, and 2.7 nm, respectively. The experimental photoluminescence spectra at each value of the average radius $\langle R\rangle$ refer to different time intervals between the pumping pulse (of duration 2.5 ps) and the measurement, the upper curve corresponding to the time interval equal to 0. According to Ref. 4, the decay of fast photoluminescence components is caused by trapping of holes onto deep (binding energy ~ 200 meV) local surface levels. Depending on the average radius of the quantum dots, the decay time varies from some tens to some hundreds of picoseconds. The separation between neighboring energy levels of a nontrapped exciton is smaller than the depth of local levels. Therefore, the relaxation in the system of ''interior'' exciton states, which have been discussed in the Introduction, can be expected to proceed more quickly than the hole trapping. This supposition is in agreement with the behavior of fast photo-

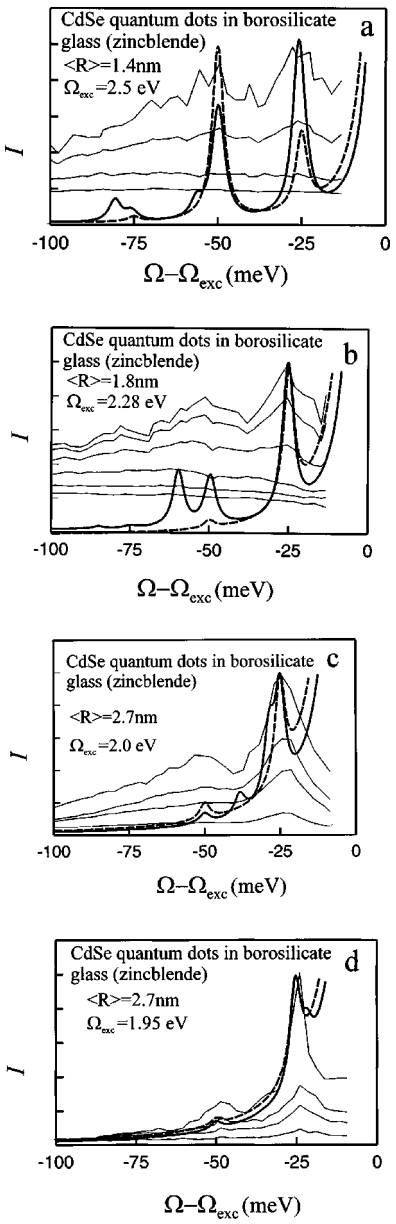

FIG. 6. Photoluminescence spectra of CdSe quantum dots embedded in borosilicate glass at different average radii and excitation energies: (a) $\langle R\rangle = 1.4$ nm, $\hbar\Omega_{exc} = 2.50$ eV; (b) $\langle R\rangle = 1.8$ nm, $\hbar\Omega_{exc} = 2.28$ eV; (c) $\langle R\rangle = 2.7$ nm, $\hbar\Omega_{exc} = 2.00$ eV; and (d) $\langle R\rangle = 2.7$ nm, $\hbar\Omega_{exc} = 1.95$ eV. Thin solid lines represent the families of experimental time-resolved photoluminescence spectra of Ref. 4 measured at different time intervals between the pumping pulse and the measurement, the upper curve corresponding to the time interval equal to 0. Theoretical results are displayed for the equilibrium-photoluminescence spectra of Eq. (33) (heavy solid lines) and for the photoluminescence spectra of Eq. (34) in the case of slow relaxation of the exciton energy (dashed lines).

luminescence components under the excitation by light whose frequency lies near the absorption band maximum (no size-selective excitation). In this case a significant shift of the photoluminescence intensity maximum from the excitation frequency appears 10 ps after the excitation pulse.[4] Therefore, it is the limiting case of the equilibrium photoluminescence rather than the opposite case of $\tau_0 \gg \tau$ that seems to be relevant to the experimental data of Ref. 4.

The quantum dots in glass are characterized by broad distribution functions over the radii R.[12,13] Therefore, even under size-selective excitation some excitons are generated in states with relatively high energy [first of all, in the states $(1S,2S_{3/2})$, $(1S,1P_{5/2})$, $(1S,1D_{5/2})$ whose energies differ slightly from each other]. In the case of equilibrium photoluminescence, the radiationless relaxation of such excitons into the lowest states $(1S,1S_3/2)$ leads to the appearance of zero-phonon luminescence peaks shifted from Ω_{exc} to lower frequencies. These peaks hide the phonon satellites [see Fig. 6(c)]. This effect becomes less pronounced when the excitation is deeper in the absorption band tail [see Fig. 6(d)].

VI. CONCLUSION

We have shown in this paper that, due to the nonadiabaticity of the exciton-phonon system in spherical quantum dots, different *channels* of the phonon-assisted optical transitions open. First, distinct from the adiabatic theory, which describes only phonon transitions through intermediate exciton states coinciding with either its initial or its final state, the present approach takes into consideration also *additional* phonon transitions: (i) between different exciton states belonging to the same degenerate level (proper Jahn-Teller effect) and (ii) between exciton states of different energy (pseudo-Jahn-Teller effect). Second, in contrast to the works based on the theory of Pekar and of Huang and Rhys, which adequately account for the adiabatic phonons only, the present approach enables one to correctly describe the transitions involving *all* types of phonons, including Jahn-Teller phonons.

The effect of the channels studied here leads to a considerable enhancement of the phonon-assisted transition probabilities in the photoluminescence of quantum dots even with relatively weak electron-phonon coupling strength. The resulting multiphonon optical spectra are considerably different from the Franck-Condon progression. In order to obtain agreement between theory and experiment, it is necessary to take into account these channels of the phonon-assisted optical transitions.

ACKNOWLEDGMENTS

The authors wish to thank Professor F. Henneberger for fruitful discussions. This work has been supported by the Interuniversity Poles of Attraction Program—Belgian State, Prime Minister's Office—Federal Office for Scientific, Technical and Cultural Affairs; Bijzonder Onderzoeksfonds (BOF); PHANTOMS Research Network; FWO-V Project No. G.0287.95 and WOG Project No. 0073.94N. V.M.F. and V.N.G. were supported by BOF NOI ''Thermodynamica van interagerende identieke deeltjes met behulp van padintegralen.'' S.N.K. and S.N.B. acknowledge with gratitude the kind hospitality received during their visit to UIA in the framework of the common Research Project No. 11-3251 supported by PHANTOMS.

APPENDIX

The shape of the absorption band edge of a spherical quantum dot is considered using the spherical model[18–20] of the exciton Hamiltonian. To zeroth order in the electron-hole

interaction the exciton ground state is fourfold degenerate with respect to the z component of the hole angular momentum F_z (see Ref. 20). The twofold spin degeneracy of the electron ground state is not important for the analysis of the Jahn-Teller effect.[26] The wave functions of the exciton ground state can be written as[20]

$$|F_z\rangle=\psi_0(r_e)\left|\frac{1}{2},\sigma_z\right\rangle\left(f_0(r_h)\left|0,\frac{3}{2},\frac{3}{2},F_z\right\rangle + g_0(r_h)\left|2,\frac{3}{2},\frac{3}{2},F_z\right\rangle\right), \tag{A1}$$

where $\psi_0(r_e)$ is the envelope wave function of an electron in the ground state, $|\frac{1}{2},\sigma_z\rangle$ is the Bloch wave function at the bottom of the conduction band, $|L,J,F,F_z\rangle$ are the eigenfunctions of the total angular momentum of a hole, and L and $J=\frac{3}{2}$ are the eigenvalues of the orbital angular momentum of a hole and its spin angular momentum, respectively. An exciton in the ground state interacts only with s phonons ($l=0$) and d phonons ($l=2$) [see Eqs. (39)–(42)]. Using Eq. (3) with Eqs. (38)–(42), one obtains

$$\mathbf{H}_{int}=\mathbf{I}\sum_{n=0}^{\infty}c_{n0}^{(B)}a_{n00}^{(B)}+\sum_{m=-2}^{2}\mathbf{V}_m\left(c_2^{(I)}a_{2m}^{(I)}+\sum_{n=0}^{\infty}c_{n2}^{(B)}a_{n2m}^{(B)}\right)+\text{H.c.}, \tag{A2}$$

where

$$c_{n0}^{(B)}=\frac{1}{\sqrt{4\pi}}\int_0^{\infty}dr v_{n0}^{(B)}(r)[\psi_0^2(r)-f_0^2(r)-g_0^2(r)], \tag{A3}$$

$$c_{n2}^{(B)}=-\frac{1}{\sqrt{5\pi}}\int_0^{\infty}dr v_{n2}^{(B)}(r)f_0^2(r)g_0^2(r), \tag{A4}$$

$$c_2^{(I)}=-\frac{1}{\sqrt{5\pi}}\int_0^{\infty}dr v_2^{(I)}(r)f_0^2(r)g_0^2(r). \tag{A5}$$

In Eq. (A2) and below, bold letters denote operator matrices in the basis of the functions $|F_z\rangle$ ($F_z=\frac{3}{2},\frac{1}{2},-\frac{1}{2},-\frac{3}{2}$). The matrices

$$\mathbf{V}_0=\begin{pmatrix}1&0&0&0\\0&-1&0&0\\0&0&-1&0\\0&0&0&1\end{pmatrix}, \tag{A6}$$

$$\mathbf{V}_1=\mathbf{V}_{-1}^{\dagger}=\begin{pmatrix}0&\sqrt{2}&0&0\\0&0&0&0\\0&0&0&-\sqrt{2}\\0&0&0&0\end{pmatrix}, \tag{A7}$$

$$\mathbf{V}_2=\mathbf{V}_{-2}^{\dagger}=\begin{pmatrix}0&0&\sqrt{2}&0\\0&0&0&\sqrt{2}\\0&0&0&0\\0&0&0&0\end{pmatrix} \tag{A8}$$

are relevant to the interaction of an exciton with d phonons. The matrices $\mathbf{V}_m$ with different m do not commute. Therefore, the interaction Hamiltonian $\mathbf{H}_{int}$ cannot be diagonalized in the basis of the functions $|F_z\rangle$ (A1) and, in contrast to the case of the adiabatic approach, the wave function of the exciton-phonon system cannot be represented as a product of an exciton wave function with a phonon wave function. This fact expresses mathematically the internal nonadiabaticity of the exciton-phonon system.

It is convenient to introduce the effective phonon modes with the second-quantization operators

$$b_s=\frac{1}{C_s}\sum_{n=0}^{\infty}c_{n0}^{(B)}a_{n00}^{(B)}, \tag{A9}$$

$$b_{dm}=\frac{1}{C_d}\left(c_2^{(I)}a_{2m}^{(I)}+\sum_{n=0}^{\infty}c_{n2}^{(B)}a_{n2m}^{(B)}\right), \tag{A10}$$

where

$$C_s=\left[\sum_{n=0}^{\infty}(c_{n0}^{(B)})^2\right]^{1/2}, \tag{A11}$$

$$C_d=\left[(c_2^{(I)})^2+\sum_{n=0}^{\infty}(c_{n2}^{(B)})^2\right]^{1/2}. \tag{A12}$$

Using Eqs. (A2) and (A6)–(A10), the evolution operator (6) averaged over the phonon ensemble can be written in the matrix representation as

$$\langle\mathbf{U}(t)\rangle_{ph}=\langle\mathbf{U}_s(t)\rangle_{ph}\langle\mathbf{U}_d(t)\rangle_{ph}, \tag{A13}$$

where

$$\mathbf{U}_s(t)=\mathbf{I}T\exp\left\{-\frac{iC_s}{\hbar}\int_0^t dt_1[b_s(t_1)+b_s^{\dagger}(t_1)]\right\}, \tag{A14}$$

$$\mathbf{U}_d(t)=T\exp\left\{-\frac{iC_d}{\hbar}\int_0^t dt_1[\mathbf{B}(t_1)+\mathbf{B}^{\dagger}(t_1)]\right\}, \tag{A15}$$

$$\mathbf{B}=\begin{pmatrix}b_{d0}&\sqrt{2}b_{d1}&\sqrt{2}b_{d2}&0\\\sqrt{2}b_{d,-1}&-b_{d0}&0&\sqrt{2}b_{d2}\\\sqrt{2}b_{d,-2}&0&-b_{d0}&-\sqrt{2}b_{d1}\\0&\sqrt{2}b_{d,-2}&-\sqrt{2}b_{d,-1}&b_{d0}\end{pmatrix}. \tag{A16}$$

The interaction of an exciton with totally symmetrical s phonons is adiabatic and the corresponding interaction matrix is diagonal. Having averaged $\mathbf{U}_s(t)$ (A14) over the phonon ensemble, one obtains the Fourier transform of the Franck-Condon progression. The probability of a K-phonon optical transition is then proportional to $\tilde{f}_{\beta K}$ (24) with $|\beta\rangle=|F_z\rangle$.

The average $\langle\mathbf{U}_d(t)\rangle_{ph}$ is calculated by using the approach developed in Sec. II. Namely, contributions into the absorption coefficient due to transitions accompanied by a change of the number of d phonons by K are taken in account to the leading (Kth) order in the small parameter η^2 (10). At the

temperatures corresponding to the experimental conditions[1–5] ($k_BT \ll \hbar\omega_0$) one obtains

$$\langle \mathbf{U}_d(t)\rangle_{ph} = \sum_{K=0}^{\infty} \frac{1}{(K!)^2}\left(\frac{C_d}{\hbar\omega_0}\right)^{2K} \langle \mathbf{B}^K(\mathbf{B}^\dagger)^K\rangle_{ph} \exp(-iK\omega_0 t). \tag{A17}$$

Using the definition (A16), the identity

$$\mathbf{B}^2 = \mathbf{I}(b_{d0}^2 + 2b_{d1}b_{d,-1} + 2b_{d2}b_{d,-2}) \tag{A18}$$

can be verified. Taking in account Eq. (A18), the average $\langle \mathbf{U}_d(t)\rangle_{ph}$ (A17) is easily calculated:

$$\langle \mathbf{U}_d(t)\rangle_{ph} = \mathbf{I}\sum_{K=0}^{\infty} \frac{1}{K!}\left(\frac{C_d}{\hbar\omega_0}\right)^{2K} \frac{4}{3}\left(\left[\frac{K+1}{2}\right] + \frac{1}{2}\right) \times \left(\left[\frac{K+1}{2}\right] + \frac{3}{2}\right)\exp(-iK\omega_0 t), \tag{A19}$$

where $[x]$ denotes the integer part of x. Equation (25) follows immediately from Eq. (A19).

*Permanent address: Department of Theoretical Physics, State University of Moldova, Strada A. Mateevici, 60, MD-2009 Kishinev, Republic of Moldova.

† Also at Universiteit Antwerpen (RUCA), Groenenborgerlaan 171, B-2020 Antwerpen, Belgium and Technische Universiteit Eindhoven, P.O. Box 513, 5600 MB Eindhoven, The Netherlands.

[1] M. G. Bawendi, W. L. Wilson, L. Rothberg, P. J. Carroll, T. M. Jedju, M. L. Steigerwald, and L. E. Brus, Phys. Rev. Lett. **65**, 1623 (1990).

[2] M. Nirmal, C. B. Murray, D. J. Norris, and M. G. Bawendi, Z. Phys. D **26**, 361 (1993).

[3] V. Jungnickel, F. Henneberger, and J. Puls, in *22nd International Conference on the Physics of Semiconductors*, edited by D. J. Lockwood (World Scientific, Singapore, 1994), Vol. 3, p. 2011.

[4] V. Jungnickel and F. Henneberger, J. Lumin. **70**, 238 (1996).

[5] D. J. Norris, Al. L. Efros, M. Rosen, and M. G. Bawendi, Phys. Rev. B **53**, 16 347 (1996).

[6] A. P. Alivisatos, T. D. Harris, P. J. Carroll, M. L. Steigerwald, and L. E. Brus, J. Chem. Phys. **90**, 3463 (1989).

[7] M. C. Klein, F. Hache, D. Ricard, and C. Flytzanis, Phys. Rev. B **42**, 11 123 (1990).

[8] Al. L. Efros, A. I. Ekimov, F. Kozlowski, V. Petrova-Koch, H. Schmidbaur, and S. Shulimov, Solid State Commun. **78**, 853 (1991).

[9] J. J. Shiang, S. H. Risbud, and A. P. Alivisatos, J. Chem. Phys. **98**, 8432 (1993).

[10] A. Mlayah, A. M. Brugman, R. Carles, J. B. Renucci, M. Ya. Valakh, and A. V. Pogorelov, Solid State Commun. **90**, 567 (1994).

[11] G. Scamarcio, V. Spagnolo, G. Ventruti, M. Lugará, and G. C. Righini, Phys. Rev. B **53**, R10 489 (1996).

[12] S. V. Gaponenko, Fiz. Tverd. Tela (Leningrad) **30**, 577 (1996).

[13] F. Henneberger and J. Puls, in *Optics of Semiconductor Nanocrystals*, edited by F. Henneberger, S. Schmitt Rink, and E. O. Göbel (Akademie-Verlag, Berlin, 1993), p. 447.

[14] S. Nomura and T. Kobayashi, Phys. Rev. B **45**, 1305 (1992).

[15] Y. Chen, S. Huang, J. Yu, and Y. Chen, J. Lumin. **60&61**, 786 (1994).

[16] S. I. Pekar, Zh. Eksp. Teor. Fiz. **20**, 267 (1950).

[17] K. Huang and A. Rhys, Proc. R. Soc. London, Ser. A **204**, 406 (1950).

[18] N. O. Lipari and A. Baldereschi, Phys. Rev. Lett. **42**, 1660 (1970).

[19] A. Baldereschi and O. Lipari, Phys. Rev. B **8**, 2697 (1973).

[20] J. B. Xia, Phys. Rev. B **40**, 8500 (1989).

[21] D. M. Mittleman, R. W. Schoenlein, J. J. Shiang, V. L. Colvin, A. P. Alivisatos, and C. V. Shank, Phys. Rev. B **49**, 14 435 (1994).

[22] R. Englman, *The Jahn-Teller Effect in Molecules and Crystals* (Wiley, New York, 1972).

[23] A. M. Stoneham, *Theory of Defects in Solids: Electronic Structure of Defects in Insulators and Semiconductors* (Clarendon, Oxford, 1975), Chap. 17.

[24] Yu. E. Perlin and B. S. Tsukerblat, *The Effects of Electron-Vibrational Interaction on the Optical Spectra of Paramagnetic Impurity Ions* (Shtiintsa, Kishinev, 1974).

[25] Yu. E. Perlin and B. S. Tsukerblat, in *The Dynamical Jahn-Teller Effect in Localized Systems*, edited by Yu. E. Perlin and M. Wagner (Elsevier, Amsterdam, 1984), p. 251.

[26] I. B. Bersuker and V. Z. Polinger, *Vibronic Interactions in Molecules and Crystals* (Springer, Berlin, 1989).

[27] H. A. Jahn and E. Teller, Proc. R. Soc. London, Ser. A **161**, 220 (1937).

[28] V. M. Fomin, E. P. Pokatilov, J. T. Devreese, S. N. Klimin, S. N. Balaban, and V. N. Gladilin, in *Proceedings of the 23rd International Conference on the Physics of Semiconductors*, edited by M. Scheffler and R. Zimmermann (World Scientific, Singapore, 1996), p. 1461.

[29] R. Kubo, J. Phys. Soc. Jpn. **12**, 570 (1957).

[30] V. B. Berestetskii, E. M. Lifshitz, and L. P. Pitaevskii, *Relativistic Quantum Theory* (Pergamon, Oxford, 1971).

[31] R. P. Feynman, Phys. Rev. **84**, 108 (1951).

[32] M. Grundmann, J. Christen, N. N. Ledentsov, J. Böhrer, D. Bimberg, S. S. Ruvimov, P. Werner, U. Richter, U. Gösele, J. Heydenreich, V. M. Ustinov, A. Yu. Egorov, A. E. Zhukov, P. S. Kop'ev, and Zh. I. Alferov, Phys. Rev. Lett. , **74**, 4043 (1995).

[33] Yu. E. Perlin, Fiz. Tverd. Tela (Leningrad) **10**, 1941 (1968).

[34] S. N. Klimin, E. P. Pokatilov, and V. M. Fomin, Phys. Status Solidi B **184**, 373 (1994).

[35] T. Takagahara, Phys. Rev. B **47**, 4569 (1993).

[36] M. Nirmal, D. J. Norris, M. Kuno, M. G. Bawendi, Al. L. Efros, and M. Rosen, Phys. Rev. Lett. **75**, 3728 (1995).

[37] G. L. Bir and G. E. Pikus, *Symmetry and Strain-Induced Effects in Semiconductors* (Wiley, New York, 1975).

[38] Al. L. Efros, Phys. Rev. B **46**, 7448 (1992).

[39] D. J. Norris and M. G. Bawendi, Phys. Rev. B **53**, 16 338 (1996).

[40] *Semiconductors. Physics of II-VI and I-VII Compounds, Semimagnetic Semiconductors*, edited by K. H. Hellwege, Landolt-Börnstein, New Series, Group III, Vol. 17, Pt. b (Springer, Berlin, 1982).